



Research



# Characterization analyzes in the geomechanical behavior of travertine rock

Carlos Alberto Luza Huillca<sup>1</sup> · Hugo Guillermo Jiménez Pacheco<sup>1</sup> · Lilia Mary Miranda Ramos<sup>1</sup> · Pavel Kewin Delgado Sarmiento<sup>2</sup> · Victor Ludgardo Alvarez Tohalino<sup>2</sup> · Héctor Enrique Terrones Diaz<sup>2</sup> · Euripedes do Amaral Vargas Jr.<sup>3</sup>

Received: 28 March 2023 / Accepted: 19 June 2023

Published online: 17 September 2023

© The Author(s) 2023 [OPEN](#)

## Abstract

There is a fundamental interest in studying travertine rocks, and this is to understand their structure, their geomechanical behavior and other particularities in order to guarantee their proper use in different engineering and architectural applications, and thus, evaluate the sustainability of the travertines, natural resources, the stability of slopes, the preservation of cultural heritage and the mitigation of possible anthropic risks. Travertine has petrological and mechanical properties similar to carbonates from oil fields such as those found in El Presal-Brazil, which currently contain the largest hydrocarbon reserves in the world. Given the impossibility of obtaining rock samples from this deposit to carry out the study, rocks similar to these were used. The present study specifically used samples of *Lapis tiburtinus* rocks, coming from the west of the city of Tivoli in Italy and these showed resistance to uniaxial and triaxial compression, and showed mechanical resistance due to increased porosity and brittleness. The investigation carried out an analysis of the geomechanical behavior travertine through an experimental program, which includes a petrological, structural, and mechanical characterization. It was determined the travertine is mainly composed of micrite and spastic calcite without the presence of grains or allochemical cements and presents high porosity of the fenestral and vulgar type. Macro and micropores were found to be chaotically distributed in the rock and have low connectivity, which demonstrates the complexity and heterogeneity of the porous structure of Roman travertine. Uniaxial and triaxial compressive strength tests were also carried out, observing a decrease in its mechanical strength due to the increase in porosity, presenting a property of brittleness in its behavior. The results were consistent and valid for this type of rock compared to other studies; determining that there is a correct and adequate operation of the triaxial cell used in the mechanical resistance tests.

## Article Highlights

- Roman travertine presents two facies, a complex porous structure with low connectivity and average porosity of 12.59%.
- Travertine is a rock of very low resistance, influence by the porosity, and the pores collapse in the banded facies.
- The Roman travertine has a higher stiffness compared to other similar strength travertines and carbonates.

✉ Hugo Guillermo Jiménez Pacheco, [hjimenez@ucsm.edu.pe](mailto:hjimenez@ucsm.edu.pe); Carlos Alberto Luza Huillca, [cluza@ucsm.edu.pe](mailto:cluza@ucsm.edu.pe); Lilia Mary Miranda Ramos, [Imirandar@unsa.edu.pe](mailto:Imirandar@unsa.edu.pe); Pavel Kewin Delgado Sarmiento, [pdelgados@unsa.edu.pe](mailto:pdelgados@unsa.edu.pe); Victor Ludgardo Alvarez Tohalino, [vtohalino@unsa.edu.pe](mailto:vtohalino@unsa.edu.pe); Héctor Enrique Terrones Diaz, [hterrones@unsa.edu.pe](mailto:hterrones@unsa.edu.pe); Euripedes do Amaral Vargas Jr., [vargas@puc-rio.br](mailto:vargas@puc-rio.br) | <sup>1</sup>Universidad Católica de Santa María de Arequipa, Arequipa, Peru. <sup>2</sup>Universidad Nacional de San Agustín de Arequipa, Arequipa, Peru. <sup>3</sup>Departamento de Engenharia Civil, Pontifícia Universidade Católica do Rio de Janeiro PUC, Rio de Janeiro, Brazil.



SN Applied Sciences

(2023) 5:267

| <https://doi.org/10.1007/s42452-023-05420-w>

SN Applied Sciences  
A **SPRINGER NATURE** journal

**Keywords** Travertine · Porous structure characteristics · Petrological characterization · Geomechanical behavior

## 1 Introduction

Carbonates in recent years have gained importance in industry, science, and technology, it is considered that approximately 60% of hydrocarbon reserves and 40% of world gas reserves are located where carbonate rocks are found [1, 2]. Within carbonate rocks, the precipitation of calcium sulfate bicarbonates and the varieties of minerals found in them are known. One aspect that is considered in the literature is establishing the formation of bacteria in the travertine formation and consequently the abundance for the formation of deposits [3, 4]. These are found in deposits of carbonate, fractured limestone, and interbedded dolomites [5, 6], presenting conditions of heterogeneity, anisotropy, and complex porosity systems that are not well studied and are affected by natural processes [7], such as diagenesis, precipitation, fracturing, originating pore systems of different sizes, ranging from a few micrometers to several meters. Travertine is currently used in the construction industry, due to its appearance and durability, for which geological and paleoclimatic information is required [8], such as its slope stability, erosion conditions and understanding of the appearance. Physical–chemical, to achieve conservation and restoration strategies [9].

The rocks of Israeli origin show pores in limestone and dolomite concentrating stresses. According to Palchick and Hatzor [10], influencing the resistance of the rock, where the Young's Modulus and the resistance stress increase as the porosity decreases and with an increase in the incidence of pores, both the Young's modulus and the resistance decrease, therefore, the compressive strength is influenced by porosity [11, 12], being an important parameter and agreeing with the modeling of geotechnical predictions for the texture coefficient of this type of rocks [13], these parameters control the physical and mechanical response of oolitic carbonates [14, 15], controlling by the distribution of microporosity within the ooids, whose characteristics establish their mechanical resistance conditions such as grain size, internal structure and composition of the mineral present [16, 17]. Other studies carried out the analysis of petrographic and petrophysical data of different limestone lithofacies and their dolomitized equivalents within a carbonate succession with slope of a fault block, relating the distribution of fractures with the textural and mechanical properties of limestone lithofacies [18, 19].

These rocks depend on microstructural characteristics and specific resistance changes [20–22], but the range in

which each of these properties varies is very wide, which makes difficult to predict its mechanical behavior. The dispersion of this property of the rock is relevant, observing in studies that the greatest dispersion is associated with the resistance depending on the alignment of the hydro-mechanical microfractures, on the evolution of its mineralogical and volcanic geomechanical characterization [23, 24]. In addition, in the mineralogical composition of the carbonates, the presence of minerals and abundance of quartz, feldspar and mica are found, establishing conditions of reduced rock resistance [25, 26].

Likewise, physical and chemical changes are related to geomechanical behavior, the degree of alteration being influenced by the density and porosity of the rock, referred to in the literature on weathering by Pola et al. [27, 28]; they can also present areas of smectic, argillic and propylitic alteration, found in ignimbrite and andesite, established by the interaction of components found in geothermal fields [29, 30]. Another fundamental aspect is the validation of the geomechanical behavior, in reference to the formation of carbon [31] and to establish the types of rocks, such as those of the lithofacies type, that involve the characteristics whether or not they have a significant effect. in the fracture of chained dolostonic rocks, which are analogous to travertine, which would show a great dependence on the physical–mechanical properties referred to the geometry and morphology of the presence of grains and pores, which establish their relationship with the failure mode of each deposit specimen studied.

A study of the mineral composition of a fine-grained lacustrine carbonate deposit, formed of different composition, is carried out by means of X-ray diffraction (XRD) analysis; description of the microstructure such as the morphology of the minerals pyrite and calcite, through scanning electron microscopy (SEM) and that the studies give the relevance of being able to understand and characterize the travertine rocks, to later analyze the influence of the porosity and the structure of the lithofacies in its resistance to uniaxial and triaxial compressive stresses, being able to contribute significantly to engineering, geology and the conservation of cultural heritage and other related areas.

The document is divided into parts, first there is the abstract, then the introduction. Then we explain how we have carried out the experimentation, we continuously explain the results and finally the corresponding conclusions and acknowledgments.

## 2 Materials and methods

### 2.1 Materials

The rock used in this study was Lapis Tiburtinus, found in Italy, west of the city of Tivoli, Acque Albule Basin, 30 km east of Rome in the Lazio region, in the Apennine Belt Centrals [32]. The study area is bounded on the south by the Aniene River, and is surrounded by the Lucretili, Tiburtini, and Cornicolani mountains. See Fig. 1.

The deposit where this rock can be found dates from approximately 0.22 M.a. corresponding to the Middle-Upper Pleistocene, here, sedimentary rocks such as travertine preserve a composition of paleofluids and paleoprecipitation [33]. This deposit is known worldwide as one of the biggest deposits with travertine rocks of quaternary age, [34]. The travertine in this region is horizontally stratified in laterally continuous strata along a wide area of approximately 30 km<sup>2</sup> [35].

### 2.2 Methodology

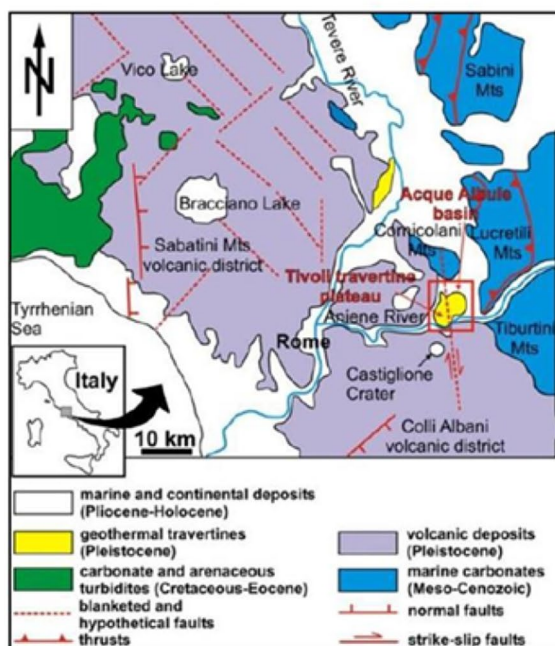
In this study, cylindrical and thin section samples were selected and prepared. To characterize the petrology, structure, and mechanical strength of the rock, the

following procedures were made: petrological, mineralogical, and chemical analyzes, X-ray tomography, and a uniaxial and triaxial compression strength test as established in the American Society for Testing and Materials—ASTM International Standard D7012-13.

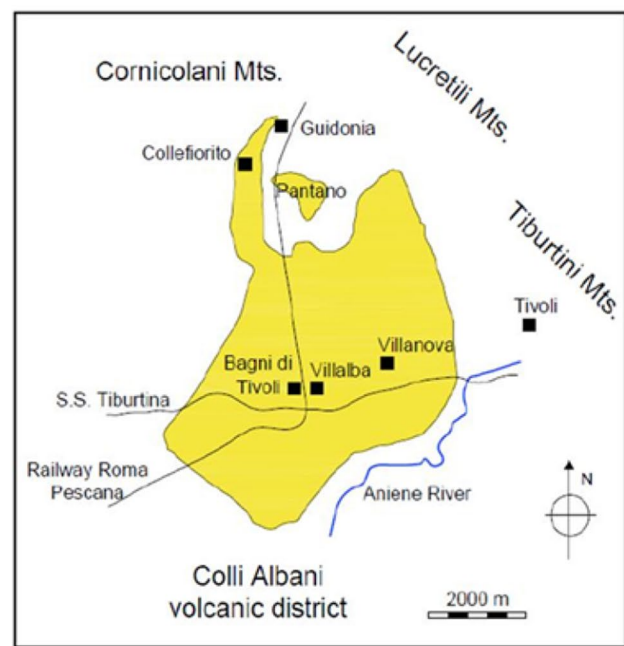
#### 2.2.1 Petrological, chemical and mineralogical characterization

Fourteen rock cylinders were drilled with 2 inches in diameter and 4 inches in length ( $L/D \approx 2$ ), and 8 thin section sheets of different directions of the travertine block were prepared. In 14 rock cylinders, the physical indexes were determined using a method established by the International Society of Rock Mechanics (ISRM) which began with the vacuum water saturation test, the test bodies were submerged in water distilled inside a desiccator and all the air was extracted with a vacuum pump for one hour, stirring every often to remove the air trapped in the rock, then the test bodies were remove and weight, this measurement was recorded with saturated mass. After that, the test bodies were placed in an oven at a constant temperature of 110 °C and weights were recorded until constant weight, which was recorded as dry mass [36].

On the other hand, four thin sheets were impregnated with a blue dye and examined in a transmitted light microscope of the Axio Skop Zeiss model. The other 4 sheets



(a)



(b)

**Fig. 1** **a** Geological Map of Central Italy in Rome, showing the location of the Tivoli Travertine Plateau, in the Acque Albule Basin. **b** map of the Acque Albule Basin and the delimitation of the study area

were metalized in gold for analysis in the scanning electron microscope (SEM) Jeol JSM—6610 Thermo Scientific brand, allowing an increase of up to 300,000X. Energy dispersive X-ray spectrometry (EDS) elemental analysis was also performed.

The mineralogical analysis was performed using three samples (M1, M2, M3) that were ground and passed through a N°. 200 sieve, and analyzed by X-ray diffraction with the D8 Discover diffractometer of the Bruker brand that allows a reading of the diffraction angle from 0° to 90°. The same samples were used for the chemical analysis carried out by dispersed energy X-ray fluorescence and elementary chemistry analysis, using the Shimadzu 800 HS spectrometer and EA 1112 elemental analyzer.

### 2.2.2 Porous structure characterization

The porous structure of the 14 drilled rock cylinders were scanned along their axial axis (4 inches), using a Micro-Tomograph V Tome × L300 of the GE/Phoenix brand provided by the Centro de Pesquisas Leopoldo Américo Miguez de Mello research unit (CENPES). A scanning was performed through X-ray computed tomography with 2D inspection (microCT) with details of up to 1 μm, generating images of 880 × 880 × 1700 pixels, with a resolution of 60 μm. These data were then processed in the Phoenix Data X 2.0 rec program. To improve the visualization of the rock phase and the porous phase, and to reduce the existing noise, the Avizo Fire 8.0 program was used to visualize the 3D images, using the Non-Local Means filter.

Geomechanical analyzes of the behaviors of rock failure mechanisms, composed of isotropic conditions at the micro-level, were compared [37]. This procedure consisted of the visualization of the digital reconstruction of the test bodies through the position of the images obtained by microtomography. After that, the porosity was determined through an image analysis performed with the "Image J" software, on each of the images, by the difference between the total volume of the test body and the volume of the solid matter scanned. It is worth mentioning that a statistical analysis was not carried out but rather a complete scan of all images for the determination of porosity.

### 2.2.3 Mechanical characterization

Uniaxial and triaxial compression tests were performed based on the ASTM D7012-13 standard. Cylindrical specimens were used for these tests, five samples were numbered: 1, 2, 3, 9 and 13 for uniaxial compression tests and six samples as: 4, 5, 6, 7, 8, 12 for axisymmetric triaxial compression tests. These tests were carried out in a high rigidity triaxial cell, designed and manufactured for the present

study, with an axial load capacity up to 2.5 MN and a radial confining pressure up to 140 MPa. To measure the axial and radial displacement, resistive strain gauges and clip-type gauges were used, applying a controlled displacement with speeds between 0.0008 and 0.0009 mm/min.

The uniaxial mechanical characterization was carried out without confinement in the triaxial cell, for which the dimensions of the test body (diameter and height) were first recorded, then it was covered with a heat shrinkable membrane, instrumented with strain gauges, placed in the interior of the triaxial cell [38] and the axial load was applied. The same procedure was followed for the triaxial test, however, the test bodies were instrumented with axial and radial displacement sensors and the axial and radial loads were applied. The data from the uniaxial and triaxial tests were recorded in an auxiliary CPU control and monitoring system using the Triaxial Rocha V1 program. The modulus of elasticity was calculated by least squares using the data from the straight section prior to the peak of the deformation curve; referred to the determination of the resistance to deformation by uniaxial compression and rock.

The uniaxial test was carried out inside the triaxial cell but without any confinement. To carry out this test, the dimensions of the test bodies whose ratio height to diameter is greater than 2 were first recorded, then the test bodies were covered by a membrane. heat-shrinkable and axial and lateral strain gauges were glued to the middle of each sample.

After the instrumentation of the test body, it is placed inside the triaxial cell, verifying the correct coupling between the test body and the plates of the triaxial cell, finally an axial load is applied. At a rate of 0.5–1 MPa/s until rupture occurs, recording the ultimate value, which is the uniaxial compressive strength.

For the execution of the triaxial test, the test bodies must have the same dimensions as for the uniaxial test. In a similar way, the test body must be covered with a heat-shrinkable membrane and instrumented with strain gauge sensors. Later, it must be placed inside the cell, verifying the correct coupling with the triaxial cell plates. In this case, the test begins by applying a hydrostatic load that consists of applying a confining and axial load of equal value but less than the uniaxial resistance, later this load can be increased to the desired value but simultaneously in both the axial and lateral axis.

The data from the uniaxial and triaxial tests were recorded in an auxiliary CPU control and monitoring system using the Triaxial Rocha V1 program. The modulus of elasticity was calculated by least squares using the data from the straight section prior to the peak of the deformation curve; referred to the determination of the resistance to deformation by uniaxial compression and rock. Young's

modulus was determined by measuring the slope of the straight line segment of the stress–strain curve. To obtain said slope, the method of least squares must be used, which allows adjusting an equation of the line, where the slope of this line is the modulus of Young.

### 3 Results

#### 3.1 Petrological, chemical and mineralogical characterization

Macroscopically, travertine is a light beige rock with high porosity of the vugular and fenestral type, it presents irregular fracture and different facies, which are: massive facies, formed by strata with thicknesses of 0.5–5 cm, normally dense with a low porosity of about 5%; Banded facie, formed by strata from 0.5 to 8 cm and characterized by areas of porosity greater than 6%. The rock presented a hardness of 3–3.5 on the Mohs scale; and generated a strong reaction to cold hydrochloric acid, indicating the presence of calcium carbonate.

According to the results of the elemental chemical analysis by X-ray fluorescence, shown in Table 1, the rock is predominantly composed of Calcium, Carbon and Oxygen (Calcite  $\text{CaCO}_3$ ), with Ca being the component with the greatest presence, also shows traces of sulfur, iron, strontium, potassium, hydrogen and nitrogen. The results obtained by X-ray diffraction show us that the rock is composed of 99.872% and 100% calcite and a non-representative part of quartz; Similar results were reported in the study conducted by Giustini et al. [39], who determined that the travertine north of Rome is composed entirely of calcite, other studies refer to rocks associated with syenite and pyroxenite with a high presence of strontium for carbonate rocks and low limestone [40–44].

**Table 1** Chemical composition of Roman travertine by X-ray fluorescence analysis

Element	M 1 (%m/m)	M 2 (%m/m)	M 3 (%m/m)
Ca	47.950	48.839	47.109
C	12.838	12.633	13.001
O	38.514	37.899	39.003
K	0.196	0.000	0.186
S	0.167	0.185	0.143
Sr	0.092	0.115	0.103
H	0.155	0.136	0.177
Fe	0.033	0.170	0.170
N	0.055	0.022	0.109
Total	100%	100%	100%
Composition	M 1 (%)	M 2 (%)	M 3 (%)

Microscopically, travertine is composed of dark gray microcrystalline or micrite calcite inside the pore, and spastic or sparitic calcite mainly on the pore surface next to the micritic structures, without the presence of allochemical grains such as ooids, oncolite, intraclasts, exhibiting a calcareous rock with diffuse contact between these components and crystalline mosaic textures, due to the fact that the sparites are larger and are observed in the form of mosaic and intersecting crystals on the inner edges of the pores [45]. The EDS analyzes and the SEM images confirmed that the rock is mainly composed of crystalline calcium carbonates, without the presence of cement between the calcite crystals as shown in Fig. 2. According to the high percentage of calcium carbonate and considering the low percentage of Magnesium found, this rock is classified as a calcitic carbonate, according to the  $\text{MgO}/\text{CaO}$  [46, 47]. Travertine, based on the relative proportions of the natural carbonate rock components can be classified as a spatic dysmicrite or mud-cement reef. The classifications of the physical and mechanical properties of the primary rocks are related to the depth at which they are found, and also to the different alterations by hydrothermal methods, using optical mineralogy that presents in the different zones of smectite, argillic and propylitic alteration.

#### 3.2 Porous structure characterization

Travertine, being a heterogeneous mineralogy rock, has a complex porous structure probably due to its genesis, showing an effective porosity between 8.4 and 14.66%, with a specific mass of 2.15–2.41  $\text{g}/\text{cm}^3$ , which reflects the complexity and heterogeneity of the porous structure of carbonates in general.

In the analysis with an optical microscope, the presence of pores of irregular geometry was observed, distributed in a dispersed way and with high density, distinguishing pores with sizes greater than 100 microns with low connectivity. See Fig. 3. Spheroid and irregular shaped pores were associated with vugular, fenestral and intercrystalline porosity [48], these have micron sizes. Microporosity is characterized by diameters less than 100  $\mu\text{m}$  and macroporosity by diameters greater than 100  $\mu\text{m}$ . Through the SEM, it was recognized that the microporosity is constituted by pores of the interparticle and intraparticulate type and without the presence of any filling in the pores. Travertine rock presents vugular type porosity but with little connectivity with the porosity conditions of the rock, manifesting as vuggy macropores that have little influence on capillary water absorption, strength, and elasticity characteristics, whose microporosity factor is a determining factor for rock resistance [49–51]. The fenestral and

**Fig. 2** **a** Calcite crystals without the presence of cement, observed through the SEM with an increase of 300,000 X; **b** Results of EDS, which indicate the predominant composition of calcium carbonate

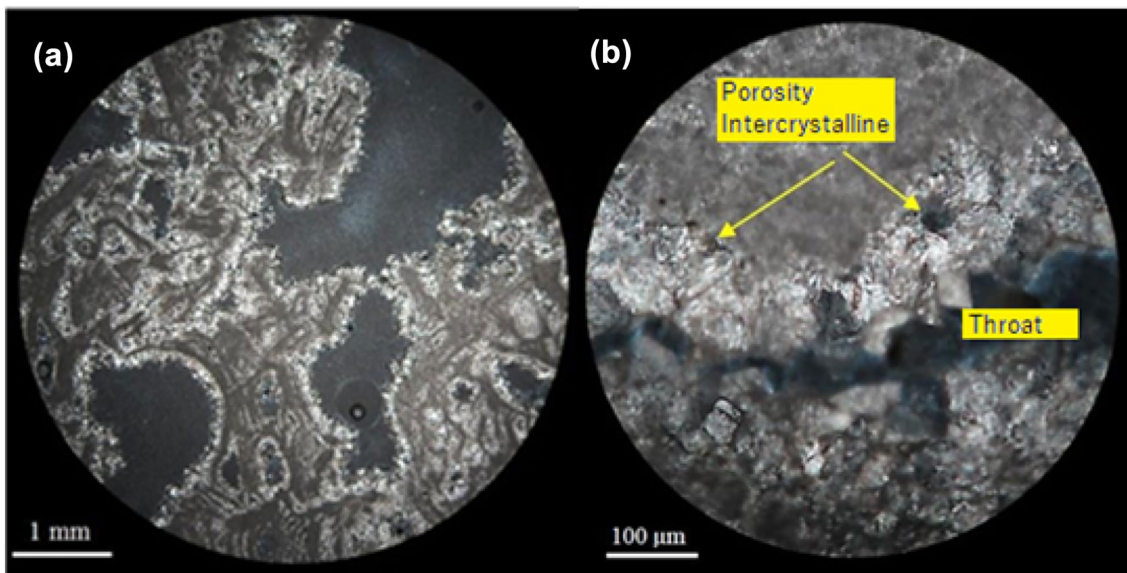
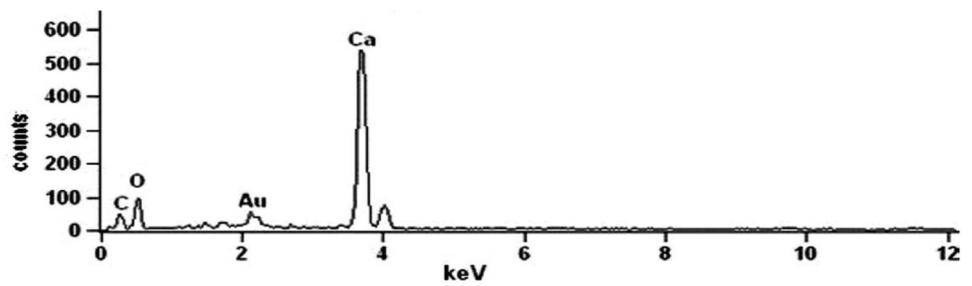
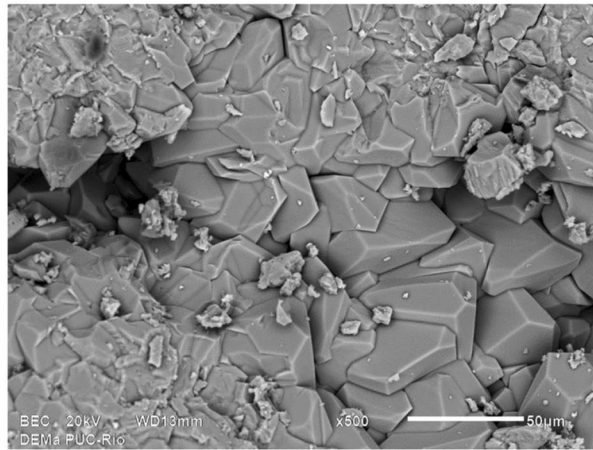


**Fig. 3** Optical microscope features: **a** scattered distribution and irregular geometry of the pores; **b** intercrystalline porosity in the spastic calcite

intercrystalline type porosity has higher connectivity, this being the type of pores registered inside of spastic calcite.

From the analysis of the two-dimensional and three-dimensional images observed through the microtomography, it is verified that the pores have a large dispersion,

presenting areas of greater density and concentration corresponding to the banded facies, apparently with low connectivity. In the images taken with the Microtomograph, it is possible to verify for each body test the existence of large pores, without contact with the surface, mainly of the vugular and fenestral type, and all this without fracturing it, being this one of the main advantages of this technique.

In the profiles of variation of the total porosity obtained from the microtomography images, strong variations can be perceived, these variations were from 3 to 23% approximately, for 12 mm of the total test bodies, demonstrating the sharp variation of the porosity in the body test, thus determining the complexity and heterogeneity of the porous structure of the travertine, since the area of

pores had to vary rapidly in a small space, this same porosity behavior is observed in each of the test bodies. See Fig. 4. A pore diameter statistic was made, where 45% corresponds to intercrystalline type porosity, 55% to vugular and fenestral type porosity. This would indicate the greater occurrence of empty spaces during their formation due to the expulsion of the gases contained within the sediments and the growth of the crystals would occur, considering that the geometry, intensity, and direction of the longest pores depend on the direction of deposition, and these are established parameters for the strength of anisotropic travertine [52, 53].

### 3.3 Mechanical characterization

The results of the Uniaxial Compressive Strength (UCS) tests are shown in Table 2, the resistance of the travertine varied between 13.26 and 48.04 MPa with a porosity of 8.40 to 14.66% respectively, determining that the mechanical resistance of the travertine is influenced by the porosity. Figure 5a shows the stress curves, this is the deformation of the travertine recorded during the axial load [54]. The stress–strain curves under uniaxial loading show a typical brittle behavior in all test bodies [42, 43, 55]. In Fig. 5b uniaxial resistance can be seen as a function of porosity, indicating a non-linear behavior characterized by a potential type curve, a similar behavior is also observed for the porosity obtained from the Image J program, these results show that the test bodies with less porosity show higher strength values, which occurs because the pores admit greater plastic deformation without exceeding the strength limit or without the pores collapsing; this occurs in test bodies with high porosity, they have low strength, and their pores collapse with small deformations. Some studies refer to the alterations generated by the increase of porosity and permeability, and the reduction of density, such as the elastic wave speed and the force, generating greater fragmentation.

The results of the Uniaxial Compression Resistance (UCS) tests are shown in Table 2, the resistance of the travertine varied between 13.26 and 48.04 MPa with a porosity of 8.40–14.66% respectively, determining that the

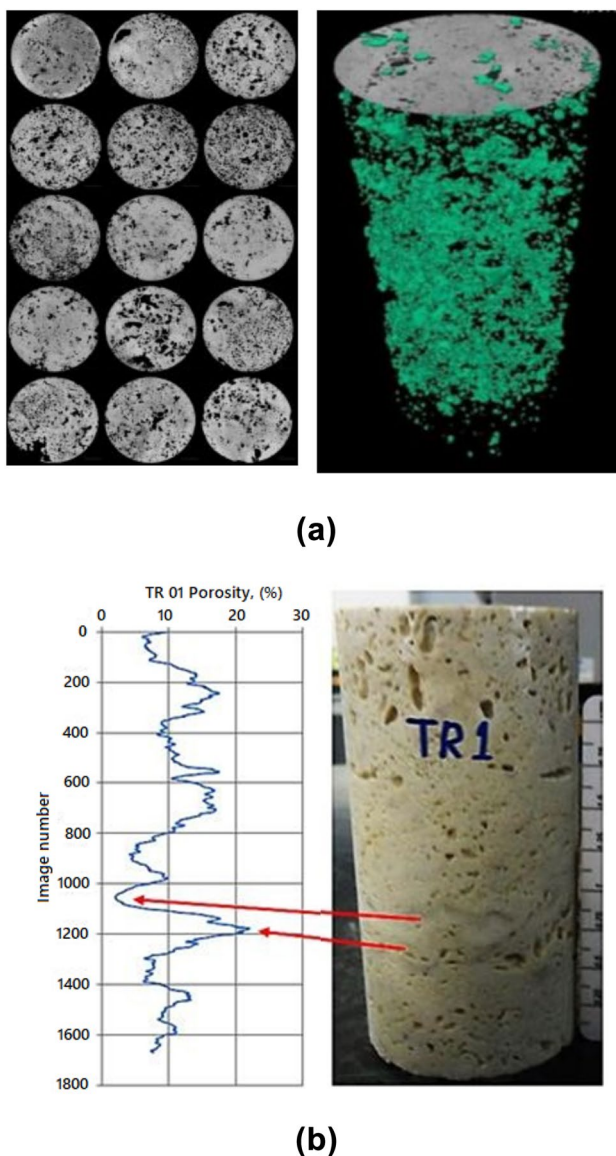


**Fig. 4** **a** Two-dimensional and three-dimensional images observed with microtomography; **b** profile of porosity variations

**Table 2** Influence of porosity vs. mechanical resistance

CP	Effective porosity (%)	UCS (MPa)	E (GPa)	Poisson ratio, ( $\nu$ )
TR 01	8.57	35.98	32.27	0.23
TR 02	8.40	48.04	39.67	0.37
TR 03	11.62	19.31	37.33	0.38
TR 09	13.21	16.32	27.57	0.22
TR 13	14.66	13.26	57.17	0.34

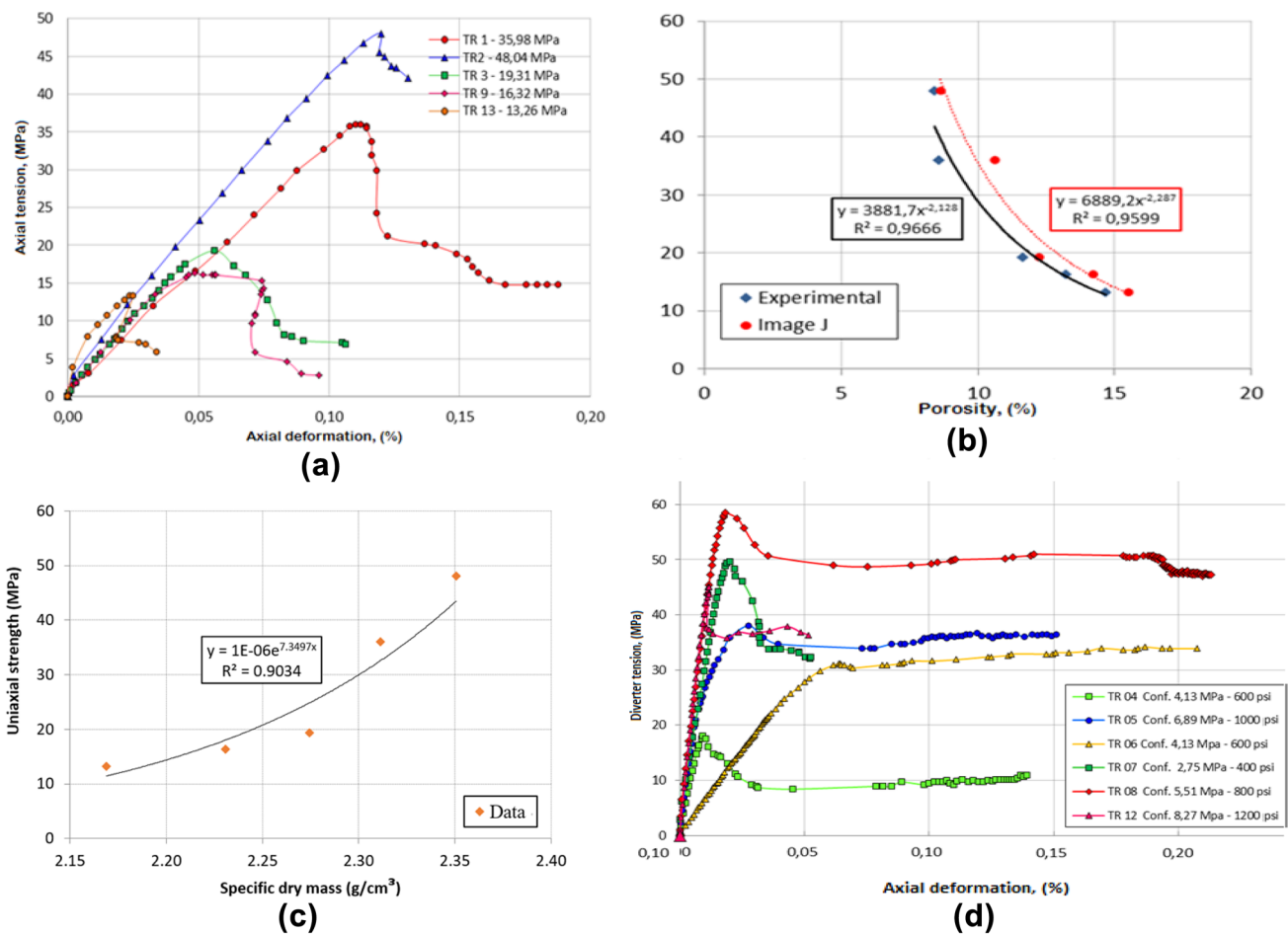


**Fig. 5** **a** Tension-deformation curve of uniaxial tests; **b** uniaxial resistance as a function of porosity; **c** uniaxial strength depending on the specific dry mass; **d** tension deformation curves of triaxial tests

mechanical resistance of the travertine is influenced by porosity; establishing that the shear modulus and the Poisson coefficient would be defined to the damping of the resistance between the applied effort and its deformation in the relationships of 0.37 and 0.34 and its deformation.

Figure 5c, shows the uniaxial strength as a function of the specific dry mass or density of the material, generating an exponential relationship between these two properties, this behavior indicates a fast increase of the uniaxial strength with a slight variation of the specific dry mass. A small variation of the pores with a diameter greater than the indicated dimension could imply a significant increase in the value of the total porosity, related to the onset of fractures due to micro defects (micropores), which indicates that the greatest concentration of stresses would be at the end of the (micropore) with a smaller radius of curvature. It was also observed that the direction of the fracture is parallel to the direction of maximum tension, but the beginning of these occurred at the tips of the pores [56].

In triaxial trials, Fig. 5d, where axial and lateral stress were applied, travertine showed an increase in strength with an increase in lateral stress of confinement stress; these results were influenced by the porosity and the greater presence of banded facies as shown in Table 3, where the test bodies with a higher percentage of porosity (greater amount of porous facies) presented collapse fracture of their pores with lower resistance values compared to the test bodies with lower porosity that presented higher strength value, and rupture of the test body due to shearing and fendilament or cracking.

Different types of rupture were identified during the tests, the test bodies with less porosity (< 12%) showed fractures of the shearing and fendilament type, while the test bodies with higher porosity (> 12%) presented fractures of the cracking or fendilament type with the occurrence of pore collapse in the banded facies, where the high porosity decreased the load area allowing the tensions to concentrate in the solid structure between the



**Table 3** Results of triaxial trials

CP	$\sigma_1$ (MPa)	$\sigma_3$ (MPa)	Voltage desv. (MPa)	E (GPa)	Poisson	CP
TR 04	22.3	4.14	18.12	22.32	0.23	12.54
TR 05	44.9	6.90	38.03	33.24	0.25	10.84
TR 06	35.3	4.14	31.13	6.10	0.44	9.38
TR 07	52.4	2.76	49.60	36.73	0.28	8.89
TR 08	64.0	5.52	58.53	36.65	0.25	9.02

pores, subsequently generating its destruction due to the increase in these tensions.

In triaxial tests, Fig. 5d, where axial and lateral stresses were applied, travertine showed an increase in strength with an increase in lateral confining stress; these results were influenced by porosity and the greater presence of banded facies as shown in Table 3, where the test bodies with the highest percentage of porosity (greater quantity of porous facies) presented fracture by collapse of their pores with resistance values lower in comparison with the test bodies with lower porosity that presented a higher resistance value, and rupture of the test body by shearing and fendilation or cracking, establishing that the property of the Poisson's ratio and its decrease to the Young's modulus, determines the deformation stress curve depending on porosity conditions, increasing its resistance.

The stress–strain curves show a brittle–ductile behavior in the different test bodies, because the graph shows a stress peak, typical of a brittle regime, followed by a drop in softening due to deformation, however it is also observed that the pressure load increases slightly as does the strain rate, which is typical of the ductile regime in porous rocks [16]. The direction of the fractures does not follow the orientation of the pore but aligns with the direction of maximum stress and the fractures begin at the type of the pores. The types of fractures observed were like those registered in the uniaxial tests with a similar porosity dependence. Considering the classification of intact rock [57], travertine is considered a rock of low to very low strength. Characteristic parameters were determined according to the strength criteria of Mohr–Coulomb, Hoek & Brown, and Kim & Lade.

Pregunta 9 Uniaxial and triaxial compression tests were performed based on ASTM Standard 7012-13. For these tests were used only cylindrical test bodies having been made five "5" uniaxial compression tests and six "6" axisymmetric triaxial compression tests. These tests were performed in a high rigidity triaxial cell, designed, and manufactured for the present study, with axial loading capacity up to 2.5 MN and radial confinement pressure up to 140 MPa. To measure the axial and radial displacement were used, resistive strain gauges y clip gauge, applying

a controlled displacement with rates between 0.0008 and 0.0009 mm/min.

## 4 Discussion

Different studies have been carried out for rocks such as Turkish travertines, Hungarians from Itaboraí in Brazil, dolomites from Turkey, and carbonates from Israel, these studies are related to our observations, they demonstrate in this way the geometry of pores, the distance, the lamination and the direction of these influence the resistance of the rock, as well as the fractures contribute to the textural mechanical properties of the carbonate rock in its dolomitization phases. [58], the travertines have heterogeneous structures, showing different geometries and pore sizes [59], the phenomena of fracturing the rock masses and pre-existing joints determine their compression referred to the geometric parameters [60].

Young's Modulus was plotted as a function of porosity. Figure 6a shows a decrease in Young's Modulus with increasing porosity, which implies that carbonates rapidly lose their stiffness with increasing porosity. It is also observed that Young's Modulus has very high values for high porosity values ( $n\% > 30\%$ ); According to the literature, when porosity is large, there is a significant impact on strength [61–63]. It is also observed that the Roman Travertine has Young's Modulus value of medium to high according to the point cloud, but the Itaboraí travertine has even higher values indicating that it is more rigid than most carbonates.

In Fig. 6b, the results of Young's Modulus versus uniaxial strength were plotted. It was observed that Roman travertine shows higher stiffness compared to other similar strength travertines and carbonates. This stiffness was higher in the travertines with pore collapse, compared to the observations made to the thermal properties that presented failures. Uniaxial compressive strength, elastic modulus parameters and Poisson's ratio are also observed [64–66]. See Table 2.

Figure 6c shows that, in general, strength decreases with the increase in porosity, such as the wide range of variation of the strength and the porosity of the carbonates.

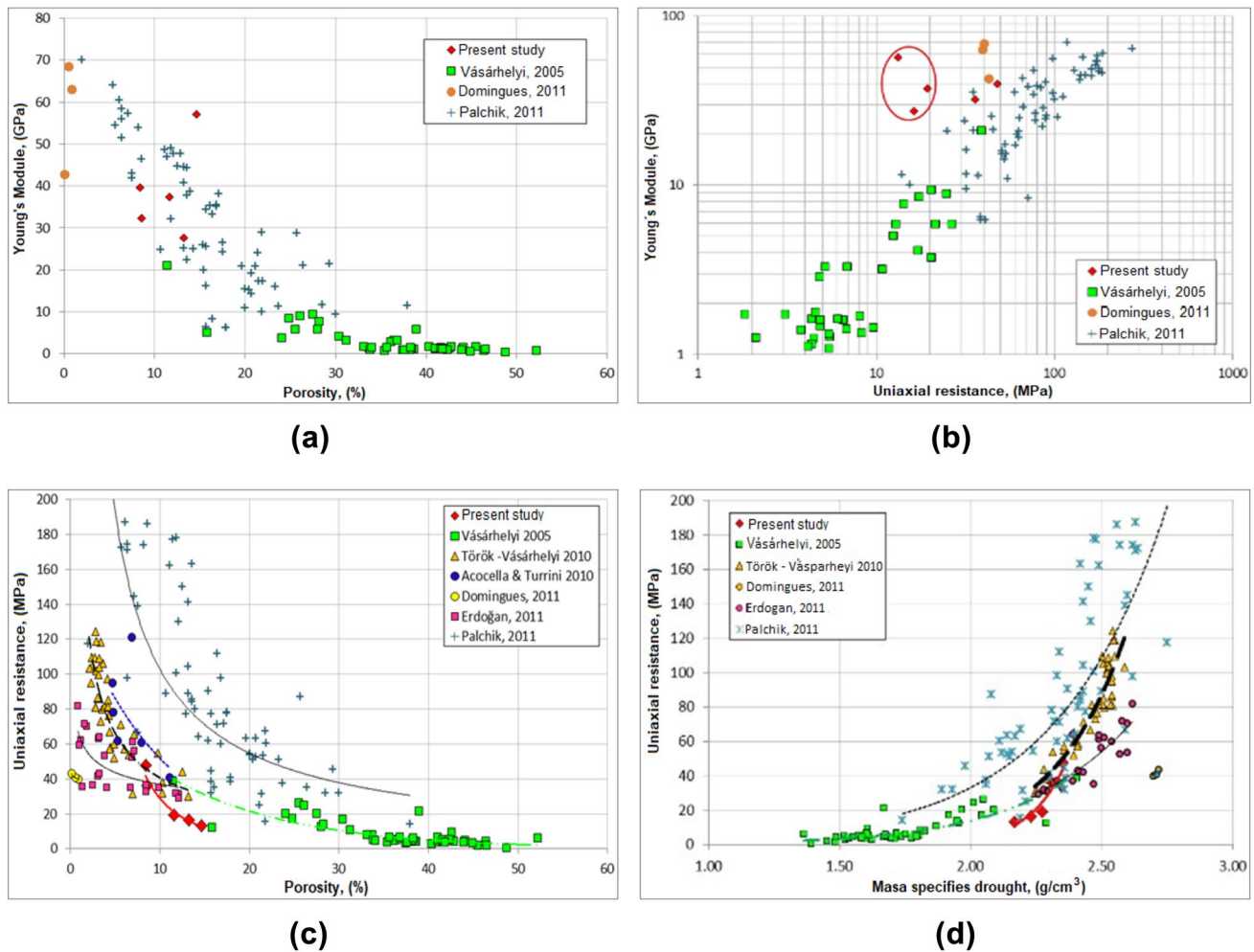


**Fig. 6** **a** Young's modulus based on porosity; **b** Young's modulus as a function of resistance; **c** uniaxial strength as a function of porosity; **d** uniaxial resistance depending on the specific mass

Being the limestones, dolomites and Chalk studied by Azimian et al. [67] that show a greater dispersion, it can also be seen that the results of the Roman Travertine are located in the area of the highest density of other travertine points, showing a good coherence of the results with other investigations [68, 69].

In Fig. 6d, different correlations are observed for the uniaxial strength referring to the dry mass of different carbonates, whose result establishes the increase in strength concerning the increase in specific dry mass; whose adjustment is observed in Itaborai travertines little distant from the point cloud, showing low resistance despite having a specific dry mass greater.

Correlation rates obtained in this study and the corresponding correlation for the different lithologies and coefficients of uniaxial strength as a function of the specific dry mass, show a good fit with the "point cloud" results, and the comparisons observed with the Itaborai travertine study in

a narrow behavior and little distance between the points found despite having a specific mass greater in the results.

## 5 Conclusions

The rock presented a complex porous structure characterized by pores of the vugular, fenestral (macropores), intraparticle and intercrystalline (micropores) type, which present low connectivity and large variations in the size, distribution and density of the pores, presenting an average porosity of 12.59%.

According to the uniaxial resistance of travertine, it is observed that it is a rock of low to very low resistance, whose mechanical properties are strongly influenced by porosity, showing that the test bodies of low porosity are more resistant, presenting fractures of the fendilation type and shear, while the high porosity rocks are less resistant,

showing fendilation type fractures with the occurrence of pore collapse mainly in their high porosity banded facies.

In triaxial compression tests, increasing the confining stress provided increased strength. This increase in strength is also dependent on porosity, as opposed to confining stress.

The travertine resistance parameters for the adjustment of the Mohr–Coulomb criterion lead to a friction angle  $\phi = 32^\circ$  and cohesion  $c = 7.561$  MPa.

For the Hoek & Brown criterion, its parameters are  $m_i = 6.072$ ,  $s = 1$ ,  $a = 0.5$  and  $C_0 = 27.056$  MPa, and for the adjustment of the Kim & Lade criterion, the following parameters are used:  $n = 2.9 \times 10^6$   $e_m = 1.42$ .

The correlations obtained with respect to other studies for different travertines and carbonates, show that for the Roman travertine the correlations are coherent and valid, observing the correct functioning of the triaxial cell used in the respective mechanical resistance tests, whose information on the geological conditions contributes to the understanding of geotechnical properties, such as compressive strength, tensile strength, modulus of elasticity, permeability, and porosity.

The characterization techniques allowed a clear and detailed interpretation of the porous systems of the rock, allowing us to predict the elastic resistivity subject to the action of decomposition agents, suggesting a better exploration of other factors that influence the deformation related to faults.

**Acknowledgements** The authors want to thank to Centro de Pesquisas Leopoldo Américo Miguez de Mello—Cenpes, which is the research department of the Petróleo Brasileiro S.A. (Petrobras); to Coordenação de Aperfeiçoamento de Pessoal de Nivel Superior—Capes for the financial support and for giving us access to their laboratories. We would also like to thank the contribution of the company Martins & Campelo of Belo Horizonte in Minas Gerais, and also to the Universidad Católica de Santa María de Arequipa and its Instituto de Investigación e Innovación en Energías Renovables y Medio Ambiente—INNOVERGY.

**Author contributions** Conceptualization: CALH, PKDS, VLAT, HETD, LMMR; Methodology: CALH, PKDS, VLAT, HETD, Investigation: CALH, LMMR, HGJP; Writing—Review and Editing: LMMR, HGJP, CALH, EdAVJ; Project administration: CALH, HGJP, HETD, Funding acquisition: CALH, HGJP, EdAVJ, Writing- original draft preparation: CALH, HGJP, EdAVJ.

**Funding** The funding was made by Centro de Pesquisas Leopoldo Américo Miguez de Mello—Cenpes, which is the research department of the Petróleo Brasileiro S.A. (Petrobras), and the Coordenação de Aperfeiçoamento de Pessoal de Nivel Superior—Capes.

**Data availability** Data is available upon request to the corresponding author.

## Declarations

**Conflict of interest** The authors have no competing interests to declare that are relevant to the content of this article.

**Consent to publish** Not applicable.

**Ethical approval** Not applicable.

**Open Access** This article is licensed under a Creative Commons Attribution 4.0 International License, which permits use, sharing, adaptation, distribution and reproduction in any medium or format, as long as you give appropriate credit to the original author(s) and the source, provide a link to the Creative Commons licence, and indicate if changes were made. The images or other third party material in this article are included in the article's Creative Commons licence, unless indicated otherwise in a credit line to the material. If material is not included in the article's Creative Commons licence and your intended use is not permitted by statutory regulation or exceeds the permitted use, you will need to obtain permission directly from the copyright holder. To view a copy of this licence, visit <http://creativecommons.org/licenses/by/4.0/>.

## References

1. Du Y, Fan T, Machel H, Gao Z (2018) Genesis of Upper Cambrian-Lower Ordovician dolomites in the Tahe Oilfield, Tarim Basin, NW China: Several limitations from petrology, geochemistry, and fluid inclusions. *Mar Pet Geol* 91:43–70. <https://doi.org/10.1016/j.marpetgeo.2017.12.023>
2. Małkowski P, Ostrowski Ł, Brodny J (2018) Analysis of Young's modulus for Carboniferous sedimentary rocks and its relationship with uniaxial compressive strength using different methods of modulus determination. *J Sustain Min* 17(3):145–157. <https://doi.org/10.1016/j.jsm.2018.07.002>
3. Chafetz HS, Folk R (1984) Travertines; depositional morphology and the bacterially constructed constituents. *J Sediment Res* 54(1):289–316. <https://doi.org/10.1306/212F8404-2B24-11D7-8648000102C1865D>
4. El Howayek A, Bobet A, Santagata M (2017) Geologic origin effects on mineralogy, index properties and fabric of a fine-grained carbonatic deposit. *Eng Geol* 216:108–121. <https://doi.org/10.1016/j.enggeo.2016.11.017>
5. Giorgioni M et al (2016) Impact of early dolomitization on multi-scale petrophysical heterogeneities and fracture intensity of low-porosity platform carbonates (Albian-Cenomanian, southern Apennines, Italy). *Mar Pet Geol* 73:462–478. <https://doi.org/10.1016/j.marpetgeo.2016.03.011>
6. Yang SQ, Yin PF, Huang YH, Cheng JL (2019) Strength, deformability and X-ray micro-CT observations of transversely isotropic composite rock under different confining pressures. *Eng Fract Mech* 214:1–20. <https://doi.org/10.1016/j.engfracmech.2019.04.030>
7. Janjuhah HT, Sanjuan J, Alqudah M, Salah MK (2020) Biostratigraphy, depositional and diagenetic processes in carbonate rocks from southern Lebanon: impact on porosity and permeability. *Acta Geol Sin Engl Ed* 95(5):1668–1683. <https://doi.org/10.1111/1755-6724.14695>
8. Li M, Zheng M, Ye C, Wang C, Zhang X, Wang X (2022) Response of Travertine dam to precipitation over the past 800 years in Zabuye Salt lake, southwestern Tibetan plateau. *Minerals* 12(7):1–15. <https://doi.org/10.3390/min12070916>

9. Khajevand R (2022) Soft computing approaches for evaluating the slake durability index of rocks. *Arab J Geosci* 15(23):2–20. <https://doi.org/10.1007/s12517-022-10997-4>
10. Palchik V, Hatzor Y (2002) Crack damage stress as a composite function of porosity and elastic matrix stiffness in dolomites and limestones. *Eng Geol* 63(3–4):233–245. [https://doi.org/10.1016/S0013-7952\(01\)00084-9](https://doi.org/10.1016/S0013-7952(01)00084-9)
11. DeBoever E, Jaramillo D, Bouvier S, Frank N, Ritzrau AS, Baumgarter L, Swennen R, Foubert A (2022) The fate of a travertine record: impact of early diagenesis on the 10 core Mammoth Hot Springs, Yellowstone national park. *Int Assoc Sedimentol* 8(1):220–250. <https://doi.org/10.1002/dep2.143>
12. Hendry J, Burgess P, Hunt D, Janson X, Zampetti V (2021) Seismic characterization of carbonate platforms and reservoirs: an introduction and review. *Geol Soc Spec Pub* 509(1):1–28. <https://doi.org/10.1144/SP509-2021-51>
13. Khajevand R (2021) Evaluating the influence of petrographic and textural characteristics on geotechnical properties of some carbonate rock samples by empirical equations. *Innov Infrastruct Solut* 6(2):1–17. <https://doi.org/10.1007/s41062-021-00498-w>
14. Regnet J, David C, Fortin J, Robion P, Makhloufi Y, Collin P (2015) Influence of microporosity distribution on the mechanical behavior of oolitic carbonate rocks. *Geomech Energy Environ* 3:11–23. <https://doi.org/10.1016/j.gete.2015.07.002>
15. Regnet JB, David C, Fortin J, Robion P, Makhloufi Y, Collin PY (2015) Geomechanics for energy and the environment influence of microporosity distribution on the mechanical behavior of oolitic carbonate rocks. *Geomech Energy Environ* 3:11–23. <https://doi.org/10.1016/j.gete.2015.07.002>
16. Baud P, Exner U, Lommatzsch M, Reuschlé T, Wong T (2017) Mechanical behavior, failure mode, and transport properties in a porous carbonate. *J Geophys Res Solid Earth* 122(9):7363–7387. <https://doi.org/10.1002/2017jb014060>
17. Firme P, Quevedo R, Roehl D, Pereira L, Cazarin C (2021) Mechanical behavior of carbonate reservoirs with single karst cavities. *Geomech Energy Environ* 25:100209. <https://doi.org/10.1016/j.gete.2020.100209>
18. Korneva I, Bastesen E, Corlett H, Eker A, Hirani J, Hollis C, Gawthorpe RL, Rotevatn A, Taylor R (2018) The effects of dolomitization on petrophysical properties and fracture distribution within rift-related carbonates (Hammam Faraun Fault Block, Suez Rift, Egypt). *J Struct Geol* 108:108–120. <https://doi.org/10.1016/j.jsg.2017.06.005>
19. Török Á, Mindszenty A, Claes H, Kele S, Fodor L, Swennen R (2017) Geobody architecture of continental carbonates: ‘Gazda’ travertine quarry (Süttő, Gerecse Hills, Hungary). *Quat Int* 437:164–185. <https://doi.org/10.1016/j.quaint.2016.09.030>
20. Mohammadi Z, Capezzuoli E, Claes H, Alipoor R, Muchez P, Swennen R (2019) Substrate geology controlling different morphology, sedimentology, diagenesis and geochemistry of adjacent travertine bodies: a case study from the Sanandaj-Sirjan zone (western Iran). *Sediment Geol* 389:127–146. <https://doi.org/10.1016/j.sedgeo.2019.06.005>
21. Pazonyi P (2014) Archaeological sites of the süttö travertine complex (Hungary) with stratigraphical and paleoecological implications from their faunas. *Quat Int* 326–327:184–190. <https://doi.org/10.1016/j.quaint.2013.05.019>
22. Pentecost A, Viles HA (2007) Review and reassessment of travertine classification. *Géographie Phys Quat* 48(3):305–314. <https://doi.org/10.7202/033011ar>
23. Pola A, Crosta GB, Fusi N, Castellanza R (2014) General characterization of the mechanical behaviour of different volcanic rocks with respect to alteration. *Eng Geol* 169:1–13. <https://doi.org/10.1016/j.enggeo.2013.11.011>
24. Bahadır Yavuz A, Rabiye Dağ SAS (2022) Quantification and estimation of the durability of stones used as construction material more precisely by modification of static rock durability index. *Constr Build Mater* 355(September):355. <https://doi.org/10.1016/j.conbuildmat.2022.129221>
25. Yusof N, Zabidi H (2016) Correlation of mineralogical and textural characteristics with engineering properties of granitic rock from Hulu Langat, Selangor. *Procedia Chem* 19:975–980. <https://doi.org/10.1016/j.proche.2016.03.144>
26. Tchouatcha MS, Kouske AP, Takojio Nguemo RE, Ganno S, Kouonang Tchounang S, Kono LD, Ngonlep Miyemack VT, Asah MF, Njinchuki DN (2018) The active thermogene travertine deposits along the Cameroon volcanic line (CVL), central africa: petrology and insights for neotectonics and paleoenvironmental approach. *J Afr Earth Sci* 144:1–16. <https://doi.org/10.1016/j.jafrearsci.2018.04.004>
27. Pola A, Crosta G, Fusi N, Barberini V, Norini G (2012) Influence of alteration on physical properties of volcanic rocks. *Tectonophysics* 566–567:67–86. <https://doi.org/10.1016/j.tecto.2012.07.017>
28. Ghasemi S, Nikudel MR, Zalooli A, Khamehchiyan M, Alizadeh A, Yousefvand F, Raeis Ghasemi AM (2022) Durability assessment of sulfur concrete and portland concrete in laboratory conditions and marine environments. *J Mater Civ Eng* 34(8):1–14. [https://doi.org/10.1061/\(asce\)mt.1943-5533.0004320](https://doi.org/10.1061/(asce)mt.1943-5533.0004320)
29. García-Del-Cura MÁ, Benavente D, Martínez-Martínez J, Cueto N (2012) Sedimentary structures and physical properties of travertine and carbonate tufa building stone. *Constr Build Mater* 28(1):456–467. <https://doi.org/10.1016/j.conbuildmat.2011.08.042>
30. Wyering LD, Villeneuve MC, Wallis IC, Siratovich PA, Kennedy BM, Gravley DM, Cant JL (2014) Mechanical and physical properties of hydrothermally altered rocks, Taupo Volcanic Zone, New Zealand. *J Volcanol Geotherm Res* 288:76–93. <https://doi.org/10.1016/j.jvolgeores.2014.10.008>
31. García-Palomo A, Macías J, Jiménez A, Tolson G, Mena M, Sánchez-Núñez J, Arce JL, Layer P, Santoyo MS, Lermo-Samaniego J (2018) NW-SE Pliocene-quaternary extension in the Apan-Aciculco region, eastern Trans-Mexican volcanic Belt. *J Volcanol Geotherm Res* 349:240–255. <https://doi.org/10.1016/j.jvolgeores.2017.11.005>
32. Faccenna C, Soligo M, Billi A, Filippis L, Funicello R, Rossetti C, Tuccimei P (2013) Late Pleistocene depositional cycles of the Lapis Tiburtinus travertine (Tivoli, Central Italy): possible influence of climate and fault activity. *Glob Planet Change* 63(4):299–308. <https://doi.org/10.1016/j.gloplacha.2008.06.006>
33. De Filippis L, Anzalone E, Billi A, Faccenna C, Poncia PP, Sella P (2013) The origin and growth of a recently-active fissure ridge travertine over a seismic fault, Tivoli, Italy. *Geomorphology* 195:13–26. <https://doi.org/10.1016/j.geomorph.2013.04.019>
34. Rodríguez-berriguete A, Alonso-zarza AM, Cabrera MC, Rodríguez-gonzalez A (2012) The Azuaje travertine: an example of aragonite deposition in a recent volcanic setting, N Gran Canaria Island, Spain. *Sediment Geol* 277–278:61–71. <https://doi.org/10.1016/j.sedgeo.2012.07.010>
35. Yagiz S (2012) Comments on ‘determination of strength parameters and quality assessment of Denizli travertines (SW Turkey)’ Ibrahim Cobanoglu and Sefer Beran Celik, 129–130 (2012) 38–47. *Eng Geol* 147–148:149–150. <https://doi.org/10.1016/j.enggeo.2012.07.012>
36. Yaşar E, Erdoğan Y (2004) Estimation of rock physicomechanical properties using hardness methods. *Eng Geol* 71(3–4):281–288. [https://doi.org/10.1016/S0013-7952\(03\)00141-8](https://doi.org/10.1016/S0013-7952(03)00141-8)
37. Giwelli A, Esteban L, Piane CD, Clennell MB (2017) Fault reactivation in travertine and its impact on hydraulic transmissibility: laboratory experiments and mesoscale structures. *Pet Geosci* 23(1):92–103. <https://doi.org/10.1144/petgeo2016-025>
38. Bieniawski ZT, Bernede MJ (1979) Suggested methods for determining the uniaxial compressive strength and deformability

- of rock materials. Part 1. Suggested method for determining deformability of rock materials in uniaxial compression. *Int J Rock Mech Min Sci* 16(2):138–140. [https://doi.org/10.1016/0148-9062\(79\)91451-7](https://doi.org/10.1016/0148-9062(79)91451-7)
39. Giustini F, Brilli M, Di Salvo C, Mancini M, Voltaggio M (2020) Multidisciplinary characterization of the buried travertine body of Prima Porta (Central Italy). *Quatern Int* 568:65–78. <https://doi.org/10.1016/j.quaint.2020.10.062>
  40. Kele S, Özkul M, Fözizs I, Gökgöz A, Baykara MO, Alçiçek MC, Németh T (2011) Stable isotope geochemical study of Pamukkale travertines: new evidences of low-temperature non-equilibrium calcite-water fractionation. *Sediment Geol* 238(1–2):191–212. <https://doi.org/10.1016/j.sedgeo.2011.04.015>
  41. Ngia NR, Hu M, Gao D (2019) Tectonic and geothermal controls on dolomitization and dolomitizing fluid flows in the Cambrian-lower Ordovician carbonate successions in the western and central Tarim Basin, NW China. *J Asian Earth Sci* 172:359–382. <https://doi.org/10.1016/j.jseaes.2018.09.020>
  42. Pola A et al (2016) Geomechanical characterization of the Miocene Cuitzeo ignimbrites, Michoacán, Central Mexico. *Eng Geol* 214:79–93. <https://doi.org/10.1016/j.enggeo.2016.10.003>
  43. Pola A, Martínez-Martínez J, Macías J, Fusi N, Crosta G, Garduño-Monroy V, Núñez-Hurtado J (2016) Geomechanical characterization of the Miocene Cuitzeo ignimbrites, Michoacán, Central Mexico. *Eng Geol* 214:79–93. <https://doi.org/10.1016/j.enggeo.2016.10.003>
  44. Salminen PE, Brasier AT, Karhu JA, Melezhik VA (2014) Travertine precipitation in the Paleoproterozoic Kuetsjärvi sedimentary formation, pechenga greenstone belt NE Fennoscandian shield. *Precambrian Res* 255(P1):181–201. <https://doi.org/10.1016/j.precamres.2014.09.023>
  45. Celik M, İbrahimoglu A (2021) Characterization of travertine stones from Turkey and assessment of their durability to salt crystallization. *J Build Eng* 43:102592. <https://doi.org/10.1016/j.jobe.2021.102592>
  46. Matera PF, Ventrucci G, Zucchi M, Brogi A, Capezzuoli E, Liotta D, Yu TL, Shen C, Huntington K, Rinyu L, Kele S (2021) Geothermal fluid variation recorded by banded Ca-carbonate veins in a fault-related, fissure ridge-type travertine depositional system (Iano, southern Tuscany, Italy). *Geofluids* 2021:28. <https://doi.org/10.1155/2021/8817487>
  47. Soete J, Kleipool LM, Claes H, Claes S, Hamaekers H, Kele S, Özkul M, Foubert A, Reijmer J (2015) Acoustic properties in travertines and their relation to porosity and pore types. *Mar Pet Geol* 59:320–335. <https://doi.org/10.1016/j.marpetgeo.2014.09.004>
  48. Maryam M (2013) New classification of carbonate rocks for process-based pore-scale modeling. *SPE J* 18(02):243–263. <https://doi.org/10.2118/163073-PA>
  49. Benavente D, Pla C, Cueto N, Galvan S, Martinez-Martinez J, Garcia-del-Cura MA, Ordoñez S (2015) Predicting water permeability in sedimentary rocks from capillary imbibition and pore structure. *Eng Geol* 195:301–311. <https://doi.org/10.1016/j.enggeo.2015.06.003>
  50. Ford TD, Pedley HM (1996) A review of tufa and travertine deposits of the world. *Earth Sci Rev* 41(3–4):117–175. [https://doi.org/10.1016/S0012-8252\(96\)00030-X](https://doi.org/10.1016/S0012-8252(96)00030-X)
  51. Long Zhou Z, Cai X, Zhao Y, Chen L, Xiong C, Li X (2016) Strength characteristics of dry and saturated rock at different strain rates. *Trans Nonferrous Met Soc China* 26(7):1919–1925. [https://doi.org/10.1016/S1003-6326\(16\)64314-5](https://doi.org/10.1016/S1003-6326(16)64314-5)
  52. Khanlari G, Naseri F (2017) The prediction of compressive strength of travertines with special reference to laminae-orientation using index tests. *Geopersia* 7(2):279–299. <https://doi.org/10.22059/GEOPE.2017.226625.648296>
  53. Khanlari GR, Naseri F, Freire-Lista DM (2019) Estimating compressive and flexural strength of travertines with respect to laminae-orientation by geomechanical properties. *Bull Eng Geol Environ* 78(3):1451–1470. <https://doi.org/10.1007/s10064-017-1139-8>
  54. Nogueira MC, Velloso E, Falcão F, Moraes A, Kiewiet LH, Kager S (2016) Numerical modelling of travertine modelagem Numérica do Comportamento Mecânico de Travertino Baseada em Ensaios Geomecânicos de Plugs Verticais. [https://doi.org/10.11137/2016\\_2\\_15\\_28](https://doi.org/10.11137/2016_2_15_28)
  55. Eberhardt E, Stead D, Stimpson B (1999) Quantifying progressive pre-peak brittle fracture damage in rock during uniaxial compression. *Int J Rock Mech Min Sci* 36(3):361–380. [https://doi.org/10.1016/S0148-9062\(99\)00019-4](https://doi.org/10.1016/S0148-9062(99)00019-4)
  56. Li FB, Teng FZ, Chen JT, Huang KJ, Wang SJ, Lang XG, Ma HR, Peng YB, Shen B (2016) Constraining ribbon rock dolomitization by Mg isotopes: implications for the dolomite problem. *Chem Geol* 445:208–220. <https://doi.org/10.1016/j.chemgeo.2016.06.003>
  57. Han Z, Weatherley D, Puscasu R (2018) Projected area-based strength estimation for jointed rock masses in triaxial compression. *Comput Geotech* 104:216–225. <https://doi.org/10.1016/j.compgeo.2018.08.020>
  58. Hu M, Ngia NR, Gao D (2019) Dolomitization and hydrotectonic model of burial dolomitization of the Furongian-lower Ordovician carbonates in the Tazhong uplift, central Tarim basin, NW China: implications from petrography and geochemistry. *Mar Pet Geol* 106:88–115. <https://doi.org/10.1016/j.marpetgeo.2019.04.018>
  59. He W, Chen K, Hayatdavoudi A, Sawant K, Lomas M (2019) Effects of clay content, cement and mineral composition characteristics on sandstone rock strength and deformability behaviors. *J Pet Sci Eng* 176:962–969. <https://doi.org/10.1016/j.petrol.2019.02.016>
  60. Palchik V (2011) On the ratios between elastic modulus and uniaxial compressive strength of heterogeneous carbonate rocks. *Rock Mech Rock Eng* 44(1):121–128. <https://doi.org/10.1007/s00603-010-0112-7>
  61. Heap MJ, Villeneuve M, Kushnir ARL, Farquharson JI, Baud P, Reuschlé T (2019) Rock mass strength and elastic modulus of the Buntsandstein: an important lithostratigraphic unit for geothermal exploitation in the Upper Rhine Graben. *Geothermics* 77:236–256. <https://doi.org/10.1016/j.geothermics.2018.10.003>
  62. Vászárhelyi B (2005) Statistical analysis of the influence of water content on the strength of the miocene limestone. *Rock Mech Rock Eng* 38(1):69–76. <https://doi.org/10.1007/s00603-004-0034-3>
  63. Vu CC, Weiss J, Plé O, Amitrano D, Vandembroucq D (2018) Revisiting statistical size effects on compressive failure of heterogeneous materials, with a special focus on concrete. *J Mech Phys Solids* 121:47–70. <https://doi.org/10.1016/j.jmps.2018.07.022>
  64. Ashtari M, Mousavi SE, Cheshomi A, Khamechian M (2019) Evaluation of the single compressive strength test in estimating uniaxial compressive and Brazilian tensile strengths and elastic modulus of marlstone. *Eng Geol* 248:256–266. <https://doi.org/10.1016/j.enggeo.2018.12.005>
  65. Brotóns V, Tomás R, Ivorra S, Alarcón JC (2013) Temperature influence on the physical and mechanical properties of a porous rock: San Julian's calcarenite. *Eng Geol* 167:117–127. <https://doi.org/10.1016/j.enggeo.2013.10.012>
  66. Munoz H, Taheri A, Chanda EK (2016) Fracture energy-based brittleness index development and brittleness quantification by pre-peak strength parameters in rock uniaxial compression.

- Rock Mech Rock Eng 49:4587–4606. <https://doi.org/10.1007/s00603-016-1071-4>
67. Azimian A, Ajalloeian R, Fatehi L (2014) An empirical correlation of uniaxial compressive strength with P-wave velocity and point load strength index on marly rocks using statistical method. *Geotech Geol Eng* 32(1):205–214. <https://doi.org/10.1007/s10706-013-9703-x>
68. Ersoy H, Yağcınalp B, Arslan M, Babacan AE, Çetiner G (2016) Geological and geomechanical properties of the carbonate rocks at the eastern Black Sea region (NE Turkey). *J Afr Earth Sci* 123:223–233. <https://doi.org/10.1016/j.jafrearsci.2016.07.026>
69. Török Á, Vásárhelyi B (2010) The influence of fabric and water content on selected rock mechanical parameters of travertine, examples from Hungary. *Eng Geol* 115(3–4):237–245. <https://doi.org/10.1016/j.enggeo.2010.01.005>

**Publisher's Note** Springer Nature remains neutral with regard to jurisdictional claims in published maps and institutional affiliations.